HHS Public Access

Author manuscript

Plast Reconstr Surg. Author manuscript; available in PMC 2020 May 01.

Published in final edited form as:

Plast Reconstr Surg. 2019 May ; 143(5): 1408–1419. doi:10.1097/PRS.0000000000005531.

Dipyridamole Augments 3D Printed Bioactive Ceramic Scaffolds to Regenerate Craniofacial Bone

Christopher D. Lopez, BA[*,1,2,3], **J. Rodrigo Diaz-Siso, MD**[*,1], **Lukasz Witek, MSci PhD**[2], **Jonathan M. Bekisz, BA**[4], **Luiz F. Gil, DDS**[5], **Bruce N. Cronstein, MD**[6], **Roberto L. Flores, MD**[1], **Andrea Torroni, MD PhD**[1], **Eduardo D. Rodriguez, MD DDS**[1], and **Paulo G. Coelho, DDS PhD**[1,2]

[1]Hansjörg Wyss Department of Plastic Surgery, NYU Langone Health, New York, NY

[2]Department of Biomaterials & Biomimetics at NYU College of Dentistry, New York NY

[3]Icahn School of Medicine at Mount Sinai, New York, NY

[4]New York University School of Medicine, New York, NY

[5]Department of Dentistry, Universidade Federal de Santa Catarina, Florianópolis, Brazil

[6]Division of Translational Medicine, Department of Medicine, NYU Langone Health, New York, NY

Abstract

Purpose: Autologous bone grafts remain a standard of care for the reconstruction of large bony defects, but limitations persist. We explored the bone regenerative capacity of customized, 3D printed bioactive ceramic (3DBC) scaffolds with Dipyridamole (DIPY), adenosine A2A receptor ($A_{2A}R$) indirect agonist known to enhance bone formation.

Methods: Critical-sized bony defects (10mm height, 10mm length, full thickness) were created at the mandibular rami of rabbits (n=15). Defects were replaced by a custom-to-defect, 3DBC scaffold composed of β-tricalcium phosphate. Scaffolds were uncoated (control), collagen-coated (COLL), or immersed in 100μM Dipyridamole (DIPY). At t=8 weeks, animals were euthanized and the rami retrieved. Bone growth was assessed exclusively within scaffold pores, and evaluated by microCT/advanced reconstruction software. MicroCT quantification was calculated. Non-decalcified histology was performed. A general linear mixed model was performed to compare group means and 95% confidence intervals (CI).

Results: Qualitative analysis did not show an inflammatory response. The control and COLL groups (12.3±8.3% and 6.9±8.3% bone occupancy of free space, respectively) had less bone

Corresponding author: Christopher D. Lopez, BA, NIH/NIAMS Research Fellow, Department of Biomaterials & Biomimetics at NYU College of Dentistry & Hansjörg Wyss Department of Plastic Surgery at NYU Langone Health, New York NY, MD Candidate, Icahn School of Medicine at Mount Sinai, New York NY, 433 1st Ave room 830 New York, NY 10010, Office: 212-998-9269, christopher.lopez2@nyumc.org.

*These authors contributed equally to this work.

Financial Disclosure Statement: The authors report no proprietary or commercial interest in any product mentioned or concept discussed in this article.

This work was presented in abstract form at Plastic Surgery The Meeting 2017 and the International Craniofacial Society Biennial Meeting 2017.

growth, while the most bone growth was in the DIPY group (26.9±10.7%), a statistically significant difference ($p<0.03$ DIPY vs. control and $p<0.01$ DIPY vs. COLL). There was significantly more residual scaffold material for the COLL group relative to the DIPY group ($p<0.015$), whereas the control group presented intermediate values (non-significant relative to both COLL and DIPY). Highly cellular and vascularized intramembranous-like bone healing was observed in all groups.

Conclusion: DIPY significantly increased the 3DBC scaffold's ability to regenerate bone in a thin bone defect environment.

Introduction

Autologous bone transfer is the preferred reconstructive option for large craniomaxillary defects, but vascularized bone transfer is still limited by donor site morbidity, surgical site infection and delayed healing,[1,2] driving the need for reconstructive approaches that do not require donor tissue. Tissue engineering ideally consists of an adequate combination of regenerative cells, molecules that signal regenerative pathways, and the matrices/devices or materials that structurally facilitate growth.[3]

While a plethora of synthetic materials have been utilized as scaffolds for bone growth, calcium phosphate-based materials have gained prominence due to their established osseoconductivity, biocompatibility,[4,5] and safety profiles.[6,7] These synthetic grafts and bone substitutes are utilized in more than half of bone-grafting cases in the United States.[8] To date, applications have been limited because these devices currently lack adequate engineering manufacturing technology to address large, patient-specific bone defects. Such limitations are currently being addressed at a fast pace through bioactive ceramic fabrication with controlled structure at different length scales through robotized additive manufacturing.[9] Such technology has permitted accurate fabrication of three-dimensional overall bulk constructs based on clinical imaging that can fit and fill patient specific defects.[9,10] However, little attention has been devoted to optimizing the geometry within the bulk of 3D printed bioactive ceramic scaffolds (i.e. open lattice porosity dimension) and their effects on bone regeneration. Such dimensional effect on bone healing has been previously addressed in osseoconductive metallic devices from macro-(overall structure) to nano-geometric levels.[11] By methodically assessing surface and bulk configurations (e.g. surface treatments and macro-geometric variations), endosteal metallic implant studies have described both early and late bone morphology and property.[12] These studies concerning metallic devices have potential translation to other osseoconductive constructs such as 3D printed scaffolds, where depending on porous lattice geometry, rapid intramembranous-like healing is expected.[12,13] However, for devices presenting porous lattice interconnectivity, the challenge lies in attaining sufficient osseoconduction to achieve continuous osseointegration that can adequately bridge the margins of extensive defects.

There is a paucity of translational *in vivo* studies assessing osseoconductive principles in porous lattice-based 3D printed scaffolds[14-16] and thus the application of tissue engineering products to reconstruct large span defects has resulted in partially successful regeneration.[17] Approaches involving bioactive agents have demonstrated improved therapeutic potential

when added to a variety of matrices and 3D printed scaffold materials.[18-20] Among these, rhBMP-2 (recombinant human bone morphogenetic protein 2) is the most investigated,[21-26] including prospective studies with potentially promising results.[27] However, concerning effects of BMPs have also been reported (e.g. exuberant bone growth, osteolysis, ectopic bone formation),[28-30] warranting the investigation of alternative osteogenic bioactive molecules, such as the recently described purinergic receptor pathway.

Adenosine is a purine nucleoside that has been termed the 'retaliatory metabolite' because of its modulatory functions at almost every organ system.[31] Recently, adenosine receptor ligation has been shown to alter bone metabolism through a not fully understood modulation of osteoclast function.[32-34] Adenosine A1 receptors (A_1R) are known to contribute to osteoclast formation and A_1R deficiency results in defective CSF-1 (colony stimulating factor 1) and RANK-L (receptor activator of Nuclear Factor κ-B ligand) induced osteoclastogenesis *in vitro*.[32] Similar observations have been made in mice subjected to A1 antagonism.[32] Adenosine A2A receptor ($A_{2A}R$) agonism has been shown to inhibit osteoclastogenesis while $A_{2A}R$ antagonism has demonstrated its activation.[34] *In vitro* and *in vivo* data have also shown that osteoblast function is positively modulated by adenosine $A_{2A}R$ agonists.[35] This purinergic bone forming mechanism has been investigated in murine craniofacial defects. Calvarial defects that were created and replaced with 3D printed scaffolds coated with $A_{2A}R$ agonists in mice enhanced bone growth as effectively as BMP-2,[36] without the concerning effects of BMPs. These promising results warrant the translation of these principles to larger defects in more translational models.

This experiment utilized Dipyridamole (DIPY), an agent that blocks cellular uptake of adenosine thereby increasing extracellular adenosine levels available to stimulate $A_{2A}R$, to stimulate bone regeneration in a critically sized mandibular defect in a rabbit model. The objective of the present investigation was to assess the efficacy of custom, 3D printed bioactive ceramic scaffolds coated with a bioactive agent for bone regeneration of critically sized mandibular defects. We hypothesized that 3D printed scaffolds, when coated with the indirect $A_{2A}R$ agonist DIPY, would increase bone regeneration without concerning side effects.

Materials and Methods

Scaffolds were composed of 100% β-tricalcium phosphate (β-TCP). A total of fifteen (n=15) skeletally mature New Zealand White rabbits from Hypharm S.A.S., weighing ~3.5kg, were used to create critical-sized [37] (10mm length × 10mm width, full thickness) mandibular ramus defects.

Colloidal Gel formulation

Previously calcined and milled ceramic powders were used for the colloidal gel formulation. [38] Concentrated β-TCP phosphate colloidal gel, where the solid volume fraction ($\phi_{ceramics}$) of the ceramic was ~46%, was produced by mixing pre-calculated amounts of ceramic powder, ammonium polyacrylate (~14.5 mg/gram ceramic) (Darvan 821A; RT Vanderbilt, Norwalk, CT, USA) solution, deionized water (DI)-H_2O, hydroxypropyl methylcellulose, 7 mg per milliliter of ceramic (Methocel F4M; Dow Chemical Company, Midland, MI, USA)

and polyethylenimine, 150 to 200 mg per 30 mL of colloidal gel, (Sigma-Aldrich, St. Louis, MO, USA).[38,39]

Scaffold design, implementation, and analysis

Scaffolds were fabricated via robocasting (Aerotech Inc., Pittsburgh, PA, USA). The 3D defect-sized scaffolds (10-mm length, 10-mm width, 3mm thickness; 250 μm struts, and 330 μm pore spacing) were designed with a computer-aided design (CAD) system (RoboCAD 4.3; 3D Inks LLC, Tulsa, OK, USA) (Figure 1). The colloidal ink was loaded into a syringe (Nordson Corp., Westlake, OH, USA) and subsequently equipped with 250 μm-diameter extrusion nozzle (Nordson Corp.). 3D cuboidal scaffolds were printed in layer-by-layer fashion in a low-viscosity paraffin oil tray to prevent drying during fabrication. After completion, scaffolds were partially dried before being sintered at 400°C, 900°C, and 1100°C.[39]

In vivo rabbit model surgical procedure

Following approval of Institutional Animal Care and Use Committee at École Nationale Vétérinaire d'Alfort (Maison-Alfort, France) where the experiment was conducted, all surgeries performed used sterile surgical technique. Preoperative buprenorphine (0.02 mg/kg) and enrofloxacin (5 mg/kg) were administered subcutaneously. Rabbits were anesthetized via intramuscular administration of Ketamine (35 mg/kg) and Xylazine (5mg/kg). A 4–5 cm submandibular incision was made, and a ten-millimeter length and width, critical-sized full thickness defect[37] was created on the posterior aspect of the right ramus (See Figure, Supplemental Digital Content 1, which shows the injury model and scaffold treatment: (top, left) Intraoperative, pre-injury visualization of intact rabbit ramus (top, right) Ramus after critical-sized defect injury and replacement with β-TCP scaffold, white arrow denotes proximal aspect of scaffold, green arrow denotes distal aspect of scaffold (bottom, left) Scaffold stabilized after insertion into defect with suturing to intact ramus and medial pterygoid (bottom, right) Depiction of critical-size defect of rabbit ramus with scaffold (purple) insertion, http://links.lww.com/PRS/D413. One defect was created per rabbit, and one scaffold inserted into each. Scaffolds were separated into 3 groups: (i) control: uncoated scaffold; (ii) collagen: scaffold coated in 2% bovine collagen solution (Collagen I, Bovine; Corning Inc., Corning, NY, USA) by full immersion and incubation at 37°C for 20 minutes and subsequent cross-linking by irradiation (120 μW cm^2 for fifteen minutes); and (iii) DIPY: collagen-coated scaffold soaked in 100μM Dipyridamole (DIPY) for fifteen minutes prior to placement. Collagen served as the carrier for the Dipyridamole molecule with release kinetics previously established for at least ten days,[40] so the collagen-coated group assessed its non-contributory yet biocompatible role as a simple drug-delivery method for DIPY.

Rabbits received a control or collagen or DIPY scaffold with dimensions that precisely matched osteotomy dimensions. After placement, scaffolds were sutured to the ramus (through two 2 mm drilled sites) and medial pterygoid, and overlying soft tissue and skin closed. No additional external/internal fixation method was applied. Buprenorphine (0.01 mg/kg) and enrofloxacin (5 mg/kg) were administered subcutaneously every 12 hours for up to 48 hours post-op. Animals were given food, ad libitum, without activity restriction. No

signs of distress or illness in animals were observed after surgery. After 8 weeks, animals were euthanized via anesthetic overdose and samples removed by sharp dissection.

Sample analysis

The ramus was removed *en bloc* and excess soft tissue and bone were removed from proximal and distal regions of the surgical site. Samples were dehydrated in a series of ethanol solutions ranging from 70–100% and embedded in a methacrylate-based resin. Samples were scanned using micro-computed tomography (μCT 40, Scanco Medical, Basserdorf, Germany) with a slice resolution of 18 μm. All data were exported in DICOM format and imported into Amira 6.3 software (Visage Imaging GmbH, Berlin, Germany) for quantitative analysis of bone formation and scaffold resorption. Scaffolds were isolated in AMIRA by use of volume editing, and regions of unique density were isolated by thresholding (Figure 2). These regions of distinct density were then quantified, with bone, scaffold, and scaffold interstices (empty space or soft tissue) cumulatively making up 100% of quantified volume (Figure 3). A single user blinded to scaffold treatment completed all microCT analysis.

Bony regeneration was also measured as a function of distance from anterior to posterior. Using Amira 6.3 software six slices of the scaffold at 0.25mm thickness were selected and isolated in increments of 1.5mm starting at the deepest (most anterior aspect) scaffold-bone interface and moving superficially (posterior towards mandibular inferior border). Each slice was then assessed for presence of bone and scaffold using Adobe Photoshop CS6® (Adobe Systems Incorporated, San Jose, CA) and quantified with JVAnalysis 2014 (NYU Biomaterials & Biomimetics, New York, NY).

Histomorphology

After microCT scanning, embedded blocks were cut into serial sections across the entire scaffold in cross-section using a diamond saw (Isomet 2000, Buehler Ltd., Lake Bluff, IL, USA). Sections were ground on a grinding machine (Metaserv 3000, Buehler, Lake Bluff, IL, USA) under water irrigation with a series of SiC abrasive paper until they were ~100 μm thick, after which samples were stained in Stevenel's blue and Van Geison red to differentiate soft, connective, and bony tissues.[41-43] Histologic sections were all chosen from the approximate middle of the entire scaffold for consistency. 2-dimensional histomorphometric quantification was not performed because of its limitations in measuring 3-dimensional bone formation.

Statistical analysis

All data was assessed for normality using the Shapiro-Wilk test ($p>0.05$) prior to analysis (IBM SPSS v23, IBM Corp., Armonk, NY, USA). All quantified reconstructed image data are presented as mean values with corresponding 95% confidence intervals. Amira 3D image reconstruction percent scaffold and bone data were analyzed using a general linear mixed model approach with fixed factors of group (control, collagen, DIPY). Pairwise comparisons for groups analysis were adjusted for multiple comparisons using Least Significant Difference (LSD) method. Group random effect was selected in this analysis for the mixed model. Slice values for bone and scaffold percentages were normalized and analyzed.

Results

Qualitative histomorphologic assessment did not show an inflammatory response, and healing occurred through an intramembranous-like healing pathway, resulting in a highly cellular and vascularized bone structure in direct contact with the scaffold material and within the scaffold porous lattice structure (Figure 4A-C). Relative to the original bone thickness (measured to range from 0.5 mm–2mm thickness at different parts of the ramus except for the thicker border), scaffolds presented substantially thicker dimensions (Figure 4A-C). Histology demonstrated that bone healing occurred through the scaffold porosity, even when the lattice structure exceeded the dimensions of the original ramus bone thickness. Soft tissue presence was also noted throughout the scaffold. High magnification microscopy evaluation depicted active bone remodeling units leading to replacement of woven bone by lamellar bone surrounding vascular structures in all three groups to varying degrees, DIPY demonstrating the most bone growth and largest degree of lamellar bone formation (Figure 5A-C). Also, an irregular scaffold material surface was observed throughout the scaffold structure irrespective of what tissue type was in contact with the bioactive ceramic structure (dark stained structure).

On 3D analysis (Figure 6), there was significantly less bone growth in the control and COLL groups (12.3±8.3% and 6.9±8.3% bone occupancy of free space, respectively), compared to the DIPY group (26.9±10.7%), ($p<0.03$ DIPY vs. control and $p<0.01$ DIPY vs. COLL). Evaluation of scaffold presence resulted in a significantly higher presence of material for the COLL group relative to the DIPY group ($p<0.015$), whereas the control group presented intermediate values (non-significant relative to both COLL and DIPY). Compared to a maximum possible scaffold volume fraction of 46% (as originally designed), at eight weeks control group scaffold volume was quantified at 33.89±6.50%, collagen group at 39.77±2.55%, and DIPY group at 26.58±4.79%. Evaluation of scaffold interstices (empty space + soft tissue) depicted the highest values for the control group, followed by the COLL and DIPY groups, respectively (all non-significant).

Bone growth as a function of distance from the most anterior/deepest aspect scaffold insertion site to the most posterior/distal at the mandibular border aspect showed a decreasing trend for the DIPY group whereas bone growth presented consistent levels as a function of distance for both control and COLL groups (Figure 7). When comparison between groups are made as a function of distance, DIPY-treated scaffolds demonstrated the highest degrees of bone formation to 4.5mm distance from anterior to posterior (significant relative to other groups to the second slice at ~3mm away from the anterior bone wall). Of note, the control group demonstrated greatest bone growth at the most posterior aspect of scaffold (significant relative to DIPY, $p<0.05$; statistically homogenous relative to the intermediate values presented by the COLL group).

Discussion

An ideal approach to bone tissue engineering in a translational model has yet to be established, despite data indicating that rapid, new bone formation through osseoconductive scaffolds is both feasible and augmented with bioactive agents. This experiment assessed

modification of bone metabolism via indirect $A_{2A}R$ activation to regenerate a critical sized defect at a bony site with limited bone quantity and quality. The porous β-TCP scaffolds in this experiment conducted regeneration bridging an entire critical size defect, despite immediate return to mastication. At the 8-week *in vivo* endpoint, Dipyridamole-coated scaffolds had significantly greater bone regeneration compared to other groups, suggesting that $A_{2A}R$ may be a promising therapeutic target for rapid bone formation.

Indirect agonism of the $A_{2A}R$ can be achieved with compounds that have well-established safety profiles, such as Dipyridamole, the prophylactic anti-thrombotic and pharmacologic cardiac stress test agent. Dipyridamole increases endogenous extracellular adenosine concentrations via blockade of equilibrative nucleoside transporter 1 (ENT-1). Recently, it has gained attention as a regenerative therapeutic for bone because $A_{2A}R$ ligation has been shown to inhibit osteoclast differentiation and promote osteoblast differentiation.[36,44,45] $A_{2A}R$ stimulation with Dipyridamole has demonstrated enhanced bone growth comparable to bone morphogenetic protein-2 (BMP-2) in a murine calvarial model, without signs of the exuberant bone growth that BMPs have shown.[28-30] Ishack et al used 3D printed scaffolds similar to those in the present study to locally deliver Dipyridamole in a murine calvaria model.[46] However, the murine model is less translational. The present study challenges these tissue engineering principles in a translational, critical-sized rabbit mandibular ramus defect; compared to calvaria, which can potentially benefit from the osteogenicity of local tissues such as dura mater,[47] the osteogenicity of tissues near the ramus is not clear.[48] Furthermore, the ramus is a dynamic load-bearing mandibular subunit that is challenged through mastication and the defect created (between the masseter and medial pterygoid that were immediately brought to function after anesthesia) was used to further challenge healing.

$A_{2A}R$ ligation augmented the osseoconductive behavior that geometries of the scaffold lattice network were deliberately synthesized to elicit. Scaffold pores demonstrated rapid bone healing behavior experimentally described for healing chambers in endosteal, osseoconductive metallic implants undergoing osseointegration.[12] Similar to implant healing chambers, scaffold porosity drove directional bone regeneration through an intramembranous-like healing,[12] across an entire critical-sized defect. Continuous communication of appropriate pore size across the entire scaffold was critical; data has reported that changes in healing chamber geometries can either hasten or impede bone formation.[49] Scaffold porosity likely allows for communication between defects and key contributors of healing (e.g. blood supply).[11]

In addition to porosity, biomaterial choice is a key consideration for bone regeneration. Ideally, tissue engineering restores original bone morphology to defect sites while simultaneously resorbing foreign materials when healing structural support is no longer required. To that end, scaffold design in this experiment used 100% β-TCP instead of more commonly utilized materials, such as hydroxyapatite (HA). HA's post-implantation resorption kinetics *in vivo* has been shown to be slow, at a rate of up to 2% per year at five years.[50] In contrast, β-TCP is a material that demonstrates more rapid degradation/resorption *in vitro* and *in vivo* than HA, a feature that is desirable for achieving more rapid replacement of scaffold with bone.

Bone regeneration notably varied across experimental groups. The DIPY group demonstrated more bone regeneration (significantly) and scaffold resorption (not significantly but with lower mean values) compared to the untreated and collagen groups. All groups demonstrated new bone growth, with evidence of several bone remodeling sites, vascular supply, and both immature woven bone as well as reorganized lamellar bone. Scaffold resorption/degradation occurred across all three groups, but more robustly in the DIPY group. It has been suggested that this is due to rebounding from transient alterations in bone metabolism that A_{2A}Rs induce at bony defects: after A_{2A}R agonism facilitates osteoclast activity suppression and osteoblast activity up regulation to restore defects, normal bone homeostasis must be reestablished, thereby necessitating escalation of osteoclast function and suppression of osteoblast proliferation.[45] Our results support this, since at eight weeks the DIPY group has greater bone formation and scaffold resorption/degradation than other groups, but free space values that are not statistically different. Our results also suggest that collagen coating delivered DIPY for osteogenesis. However, collagen coating alone resulted in less bone formation within scaffold structure and less scaffold resorption/degradation, suggesting that it limits early bone remodeling. This is likely due to collagen functioning as a barrier between highly osseoconductive scaffolds and osteogenic cells that facilitate regeneration.

Theoretically, the defect's anterior regions should present the highest potential for osseoconductive influence due to its proximity with all three-defect walls. However, this only held true for the DIPY-treated scaffold group; in the absence of DIPY, control and COLL group osseoconduction arose in discrete pockets irrespective of anterior or posterior location. Only DIPY-treated scaffolds demonstrated a trend of greater bone healing at the anterior aspect of the scaffold, supporting the new but growing body of data reporting the targeting of adenosine receptors as a promising approach to new bone formation.[36,45,46,51,52]

In conclusion, Dipyridamole seems to increase bone regeneration qualitatively and quantitatively. Future directions include longer studies to determine whether DIPY-treated scaffolds can regenerate defects faster than uncoated scaffolds or if these effects are transient. Even if uncoated scaffolds can regenerate defects completely over a longer period, if Dipyridamole can expedite complete healing the benefits in terms of healthcare costs and patient quality of life will be significant. Dose-dependent effects of Dipyridamole are also critical to establish ideal regenerative dosage. Also, settings that mimic trauma and large oncologic resections are needed to assess if bone regeneration can occur local tissue support. Elucidating the cellular mechanisms involved in bone repair is also critical as Dipyridamole likely enhanced a marrow-limited osseoconductive mechanism by altering micro-environmental cues and recruiting from adjacent structures. The mechanism is likely more complicated than simply increasing stem cell recruitment and osteoblast expression, given that A_{2A}R stimulation does not actually alter osteoblast differentiation, but rather regulates the expression of proteins used in osteogenesis by osteoblasts.[45,46,52] By understanding the factors that contribute to bone regeneration, they can be targeted to address cases where bone healing mechanisms are compromised (e.g. pathologic bone disease, diabetes, etc.).

Supplementary Material

Refer to Web version on PubMed Central for supplementary material.

Acknowledgments

Funding: This work was supported by the National Institute of Arthritis and Musculoskeletal and Skin Diseases [award 5R01AR068593–02 and award supplement 3R01AR068593–02S1].

References

1. Hidalgo DA Condyle transplantation in free flap mandible reconstruction. Plastic and reconstructive surgery 93, 770–781 (1994). [PubMed: 8134436]
2. Hidalgo DA & Rekow A A review of 60 consecutive fibula free flap mandible reconstructions. Plastic and reconstructive surgery 96, 585–596 (1995). [PubMed: 7638283]
3. Langer R & Vacanti JP Tissue engineering. Science (New York, N.Y.) 260, 920–926 (1993).
4. Inzana JA et al. 3D printing of composite calcium phosphate and collagen scaffolds for bone regeneration. Biomaterials 35, 4026–4034 (2014). [PubMed: 24529628]
5. Simon JL et al. In vivo bone response to 3D periodic hydroxyapatite scaffolds assembled by direct ink writing. Journal of Biomedical Materials Research Part A 83A, 747–758, doi:10.1002/jbm.a.31329 (2007).
6. Nicholas RW & Lange TA Granular tricalcium phosphate grafting of cavitary lesions in human bone. Clinical orthopaedics and related research 306, 197–203 (1994).
7. U.S, Food and Drug Administration, H. H. S. Dental devices; reclassification of tricalcium phosphate granules and classification of other bone grafting material for dental bone repair. Final rule. Federal register 70, 21947–21950 (2005). [PubMed: 15858911]
8. Roberts TT & Rosenbaum AJ Bone grafts, bone substitutes and orthobiologics: the bridge between basic science and clinical advancements in fracture healing. Organogenesis 8, 114–124, doi:10.4161/org.23306 (2012). [PubMed: 23247591]
9. Bekisz JM et al. Dipyridamole enhances osteogenesis of three-dimensionally printed bioactive ceramic scaffolds in calvarial defects. Journal of cranio-maxillo-facial surgery : official publication of the European Association for Cranio-Maxillo-Facial Surgery, doi:10.1016/j.jcms.2017.11.011 (2017).
10. Oh TS, Jeong WS, Chang TJ & Koh KS Customized Orbital Wall Reconstruction Using Three-Dimensionally Printed Rapid Prototype Model in Patients With Orbital Wall Fracture. J Craniofac Surg. 2016;27:2020–2024. [PubMed: 28005746]
11. Coelho PG, Jimbo R, Tovar N & Bonfante EA Osseointegration: Hierarchical designing encompassing the macrometer, micrometer, and nanometer length scales. Dental Materials 31, 37–52 (2015). [PubMed: 25467952]
12. Coelho PG & Jimbo R Osseointegration of metallic devices: current trends based on implant hardware design. Archives of biochemistry and biophysics 561, 99–108 (2014). [PubMed: 25010447]
13. Liao HT, Lee MY, Tsai WW, Wang HC & Lu WC Osteogenesis of adipose-derived stem cells on polycaprolactone–β-tricalcium phosphate scaffold fabricated via selective laser sintering and surface coating with collagen type I. Journal of Tissue Engineering and Regenerative Medicine 10, E337–E353 (2016). [PubMed: 23955935]
14. Temple JP et al. Engineering anatomically shaped vascularized bone grafts with hASCs and 3D-printed PCL scaffolds. Journal of biomedical materials research Part A 102, 4317–4325 (2014). [PubMed: 24510413]
15. Bose S, Tarafder S & Bandyopadhyay A Effect of Chemistry on Osteogenesis and Angiogenesis Towards Bone Tissue Engineering Using 3D Printed Scaffolds. Annals of Biomedical Engineering, 1–12 (2016). [PubMed: 26620776]

16. Zhang W et al. Cartilage repair and subchondral bone migration using 3D printing osteochondral composites: a one-year-period study in rabbit trochlea. BioMed research international 2014 (2014).
17. Karlsson J, Egol KA, Jazrawi LM & Coelho PG Multilayer scaffolds in orthopaedic tissue engineering. Knee Surgery, doi:10.1007/s00167-014-3453-z (2016).
18. Chen X, Zhao Y, Geng S & Miron RJ In vivo experimental study on bone regeneration in critical bone defects using PIB nanogels/boron-containing mesoporous bioactive glass composite scaffold. Int J Nanomedicine 2015;10:839–846. [PubMed: 25653525]
19. Zhang J et al. Three-dimensional printing of strontium-containing mesoporous bioactive glass scaffolds for bone regeneration. Acta biomaterialia (2014).
20. van der Stok J, Wang H & Yavari AS Enhanced bone regeneration of cortical segmental bone defects using porous titanium scaffolds incorporated with colloidal gelatin gels for time-and dose-controlled delivery of dual growth factors. Tissue Eng Part A 2013;19:2605–2614. [PubMed: 23822814]
21. Ribeiro FO, Gómez-Benito M, Folgado J, Fernandes PR & García-Aznar J In silico mechano-chemical model of bone healing for the regeneration of critical defects: the effect of BMP-2. PloS one 10, doi:10.1371/journal.pone.0127722 (2015).
22. Wehrhan F, Amann K, Molenberg A, Lutz R, Neukam FW, Schlegel KA. PEG matrix enables cell-mediated local BMP-2 gene delivery and increased bone formation in a porcine critical size defect model of craniofacial bone regeneration. Clin Oral Implants Res. 2012;23:805–813. [PubMed: 22151397]
23. Laurencin CT, Attawia MA, Lu LQ, Borden MD & Lu HH Poly (lactide-co-glycolide)/ hydroxyapatite delivery of BMP-2-producing cells: a regional gene therapy approach to bone regeneration. Biomaterials (2001).
24. Fu YC, Nie H, Ho ML, Wang CK, Wang CH. Optimized bone regeneration based on sustained release from three-dimensional fibrous PLGA/HAp composite scaffolds loaded with BMP-2. Biotechnol Bioeng. 2008;99:996–1006. [PubMed: 17879301]
25. Lee SS, Huang BJ, Kaltz SR, Sur S & Newcomb CJ Bone regeneration with low dose BMP-2 amplified by biomimetic supramolecular nanofibers within collagen scaffolds. Biomaterials (2013).
26. Lee JW, Kang KS, Lee SH, Kim JY, Lee BK, Cho DW. Bone regeneration using a microstereolithography-produced customized poly (propylene fumarate)/diethyl fumarate photopolymer 3D scaffold incorporating BMP-2 loaded PLGA microspheres. Biomaterials 2011;32:744–752. [PubMed: 20933279]
27. Liang F et al. Three-Dimensional Cone Beam Computed Tomography Volumetric Outcomes of rhBMP-2/Demineralized Bone Matrix versus Iliac Crest Bone Graft for Alveolar Cleft Reconstruction. Plastic and reconstructive surgery 140, 767–774, doi:10.1097/PRS.0000000000003686 (2017). [PubMed: 28953728]
28. Carragee EJ, Hurwitz EL & Weiner BK A critical review of recombinant human bone morphogenetic protein-2 trials in spinal surgery: emerging safety concerns and lessons learned. The Spine Journal 11, 471–491 (2011). [PubMed: 21729796]
29. Spiro AS et al. BMP-7–induced ectopic bone formation and fracture healing is impaired by systemic NSAID application in C57BL/6-mice. Journal of Orthopaedic Research 28, 785–791 (2010). [PubMed: 20063306]
30. Kinsella CR Jr et al. Recombinant Human Bone Morphogenetic Protein-2–Induced Craniosynostosis and Growth Restriction in the Immature Skeleton. Plastic and reconstructive surgery 127, 1173–1181 (2011). [PubMed: 21364420]
31. Newby AC Adenosine and the concept of ‘retaliatory metabolites’. Trends in Biochemical Sciences 9, 42–44 (1984).
32. Kara FM et al. Adenosine A1 receptors regulate bone resorption in mice: Adenosine A1 receptor blockade or deletion increases bone density and prevents ovariectomy-induced bone loss in adenosine A1 receptor–knockout mice. Arthritis & Rheumatism 62, 534–541, doi:10.1002/art.27219 (2010). [PubMed: 20112380]

33. Mediero A et al. Adenosine A2A receptor activation prevents wear particle-induced osteolysis. Sci Transl Med 4, 135ra165, doi:10.1126/scitranslmed.3003393 (2012).
34. Mediero A, Kara FM, Wilder T & Cronstein BN Adenosine A(2A) receptor ligation inhibits osteoclast formation. The American journal of pathology 180, 775–786, doi:10.1016/j.ajpath.2011.10.017 (2012). [PubMed: 22138579]
35. Mediero A, Wilder T, Perez-Aso M & Cronstein BN Direct or indirect stimulation of adenosine A2A receptors enhances bone regeneration as well as bone morphogenetic protein-2. FASEB journal : official publication of the Federation of American Societies for Experimental Biology 29, 1577–1590, doi:10.1096/fj.14-265066 (2015). [PubMed: 25573752]
36. Mediero A et al. Ticagrelor regulates osteoblast and osteoclast function and promotes bone formation in vivo via an adenosine-dependent mechanism. The FASEB Journal 30, 3887–3900 (2016). [PubMed: 27511945]
37. Shah SR et al. A composite critical-size rabbit mandibular defect for evaluation of craniofacial tissue regeneration. Nature Protocols 11, 1989–2009 (2016). [PubMed: 27658014]
38. Witek L et al. Sintering effects on chemical and physical properties of bioactive ceramics. Journal of Advanced Ceramics 2, 274–284 (2013).
39. Szpalski C et al. Bony engineering using time-release porous scaffolds to provide sustained growth factor delivery. Journal of Craniofacial Surgery 23, 638–644 (2012). [PubMed: 22565873]
40. Mediero A et al. Ticagrelor regulates osteoblast and osteoclast function and promotes bone formation in vivo via an adenosine-dependent mechanism. FASEB journal : official publication of the Federation of American Societies for Experimental Biology 30, 3887–3900, doi:10.1096/fj.201600616R (2016). [PubMed: 27511945]
41. Cerro DM, Cogen J & Cerro DC Stevenel's Blue, an excellent stain for optical microscopical study of plastic embedded tissues. Microscopica acta 83, 117–121 (1980). [PubMed: 6156384]
42. Jensen LN, Jensen JS, Gotfredsen K. A method for histological preparation of undecalcified bone sections containing acrylic bone cement. Biotech Histochem. 1991;1:82–86. [PubMed: 1714768]
43. Jensen LN & Jensen JRS A method for histological preparation of undecalcified bone sections containing acrylic bone cement. Biotechnic & histochemistry, doi:10.3109/10520299109110555 (1991).
44. Mediero A, Kara FM, Wilder T & Cronstein BN Adenosine A 2A receptor ligation inhibits osteoclast formation. The American journal of pathology 180, 775–786 (2012). [PubMed: 22138579]
45. Mediero A, Wilder T, Perez-Aso M & Cronstein BN Direct or indirect stimulation of adenosine A2A receptors enhances bone regeneration as well as bone morphogenetic protein-2. The FASEB Journal 29, 1577–1590 (2015). [PubMed: 25573752]
46. Ishack S, Mediero A, Wilder T, Ricci JL & Cronstein BN Bone regeneration in critical bone defects using three-dimensionally printed β-tricalcium phosphate/hydroxyapatite scaffolds is enhanced by coating scaffolds with either dipyridamole or BMP-2. Journal of Biomedical Materials Research Part B: Applied Biomaterials (2015).
47. Moore WR, Graves SE, Bain GI. Synthetic bone graft substitutes. ANZ J Surg. 2001;71:354–361. [PubMed: 11409021]
48. Seale P & Rudnicki MA A new look at the origin, function, and "stem-cell" status of muscle satellite cells. Developmental biology 218, 115–124 (2000). [PubMed: 10656756]
49. Marin C et al. Histomorphologic and histomorphometric evaluation of various endosseous implant healing chamber configurations at early implantation times: a study in dogs. Clinical oral implants research 21, 577–583 (2010). [PubMed: 20105196]
50. Moore WR, Graves SE & Bain GI Synthetic bone graft substitutes. ANZ J Surg 71, 354–361 (2001). [PubMed: 11409021]
51. Holmes D Bone: Antiplatelet agent promotes bone formation. Nature Reviews Endocrinology 12, 626–626 (2016).
52. Mediero A & Cronstein BN Adenosine and bone metabolism. Trends in Endocrinology & Metabolism 24, 290–300 (2013). [PubMed: 23499155]

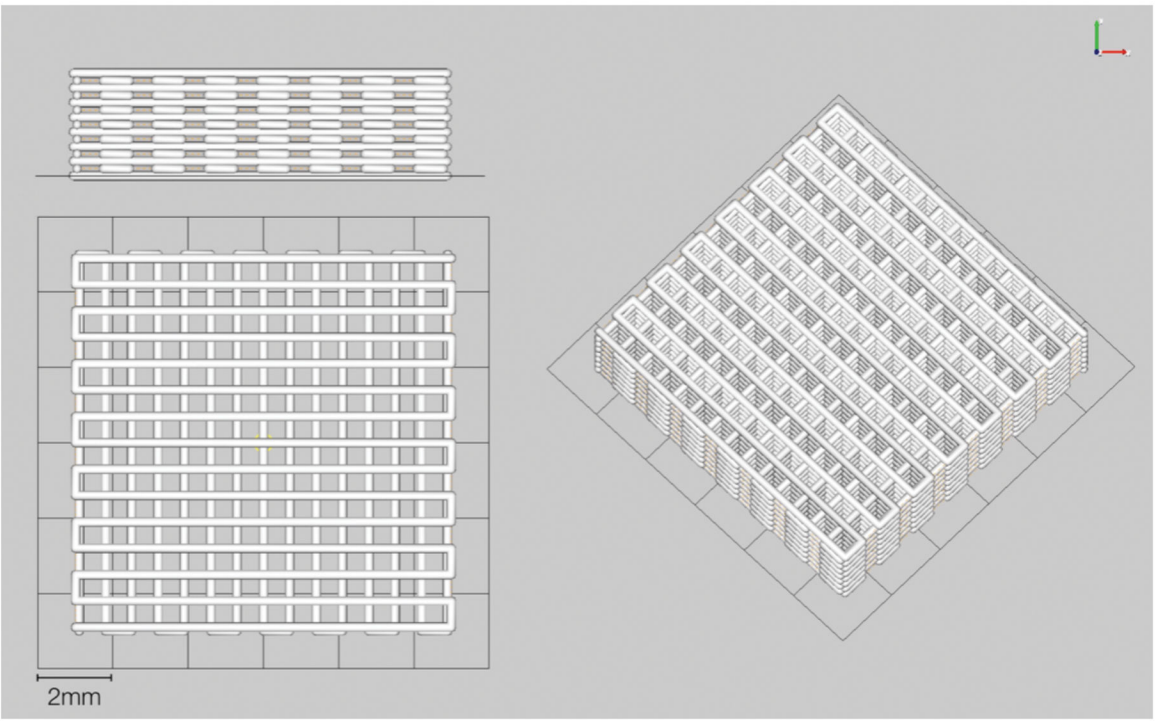

Figure 1:
Computer-aided design (CAD) scaffold 10mm length, 10mm width, 3mm thickness (a) 3mm thick side view (b) 10mm × 10mm front view and (c) Iso view

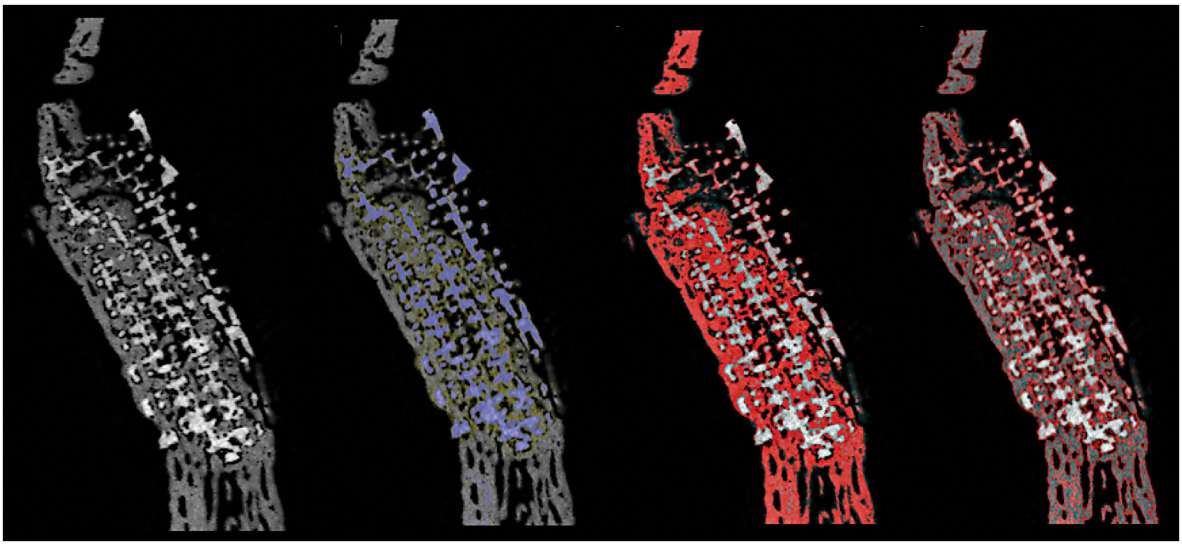

Figure 2:

Micro CT Slice Thresholding of Bone & Scaffold

a)MicroCT slice of ramus: scaffold with new bone formation throughout porosity in continuity with native bone. b) MicroCT slice of ramus with scaffold isolated by thresholding, with selection highlighted in blue c) MicroCT slice with bone isolated by thresholding, with selection highlighted in red. d) MicroCT slice with thresholded bone outlined in red.

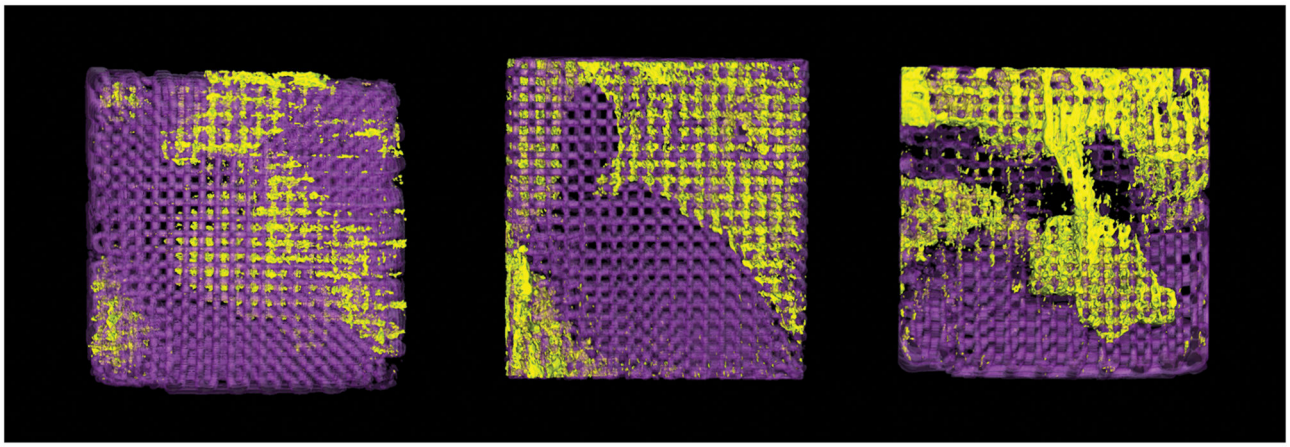

Figure 3:

3D reconstruction of scaffolds with new bone growth exclusively within scaffold porosity. Scaffold is in purple, new bone is in yellow.

(a) Control group (b) Collagen-coated group and (c) Dipyridamole experimental group.

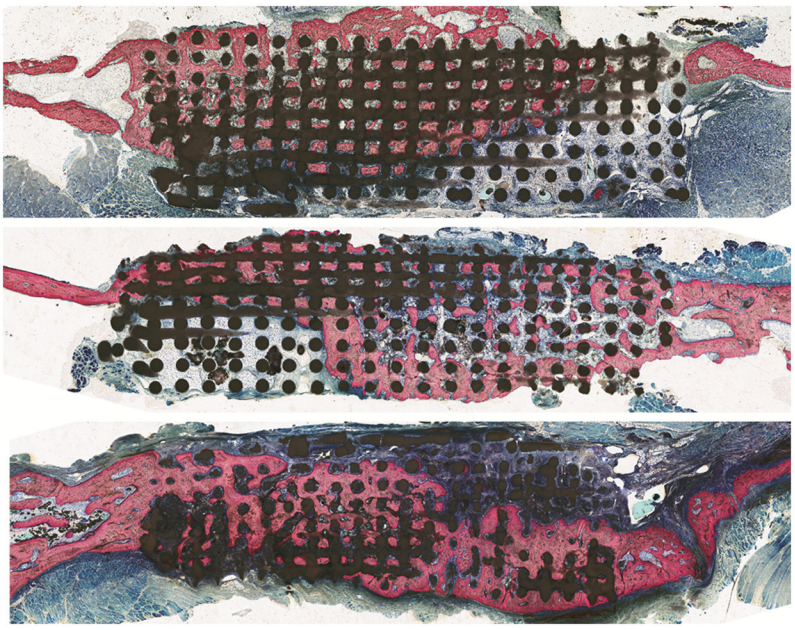

Figure 4:

Histology

Optical micrographs of scaffold inserted into ramus after 8 weeks. Bone (pink) on either side of scaffold depicts original ramus bone thickness and scaffold (black) demonstrates directional bone growth throughout porosity.

a) control group b) COLL group c) DIPY group.

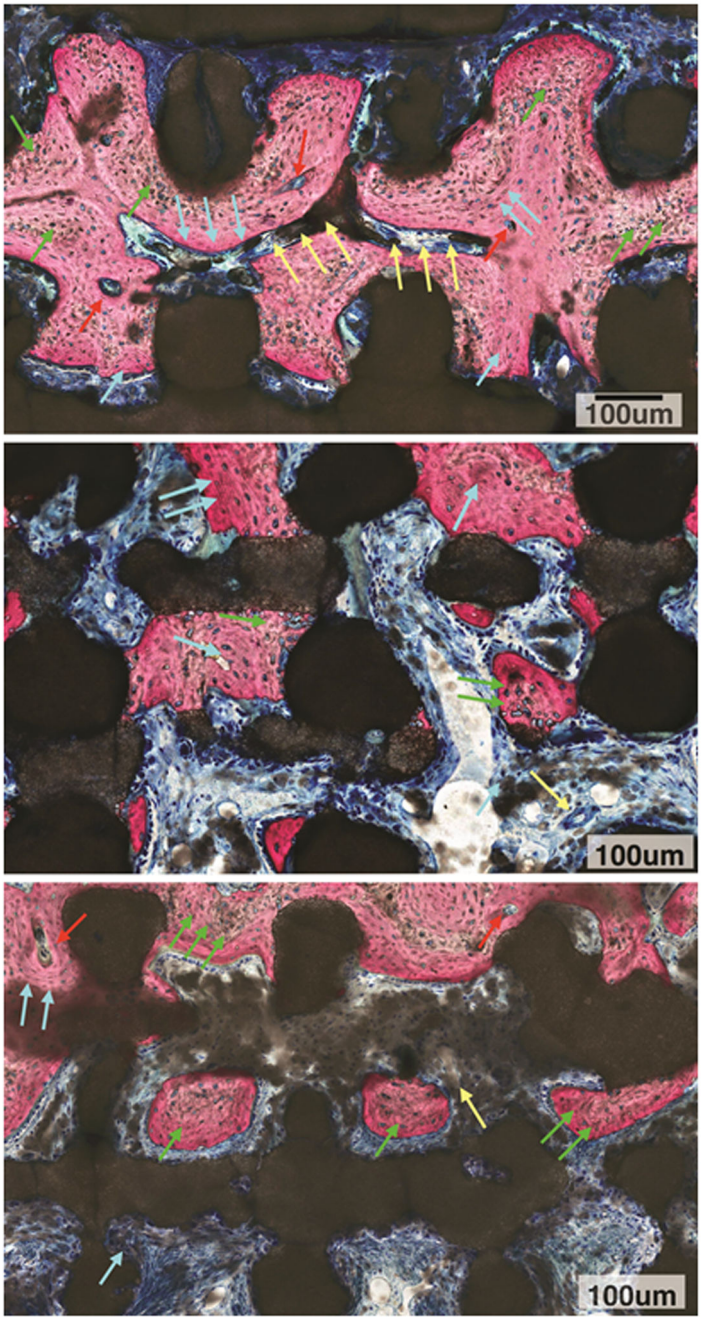

Figure 5A:

High magnification microscopy evaluation of DIPY group depicted active bone remodeling units (red arrows) leading to replacement of woven bone (green arrows) by lamellar bone (blue arrows) surrounding vascular structures (yellow arrows). Also, an irregular scaffold material surface was observed throughout the scaffold structure irrespective of what tissue type was in contact with the bioactive ceramic structure (dark stained structure).

5B: High magnification microscopy evaluation of COLL group depicted woven bone (green arrows) and replacement with lamellar bone (blue arrows). Also, irregular scaffold material

surface was observed throughout the scaffold structure irrespective of what tissue type was in contact with the bioactive ceramic structure (dark stained structure).

5C: High magnification microscopy evaluation of control group depicted woven bone (green arrows) with some replacement by lamellar bone (blue arrows) in the presence of an active bone remodeling unit (red arrows), Vascular structure is depicted as well (yellow arrow). An irregular scaffold material surface was observed throughout the scaffold structure irrespective of what tissue type was in contact with the bioactive ceramic structure (dark stained structure).

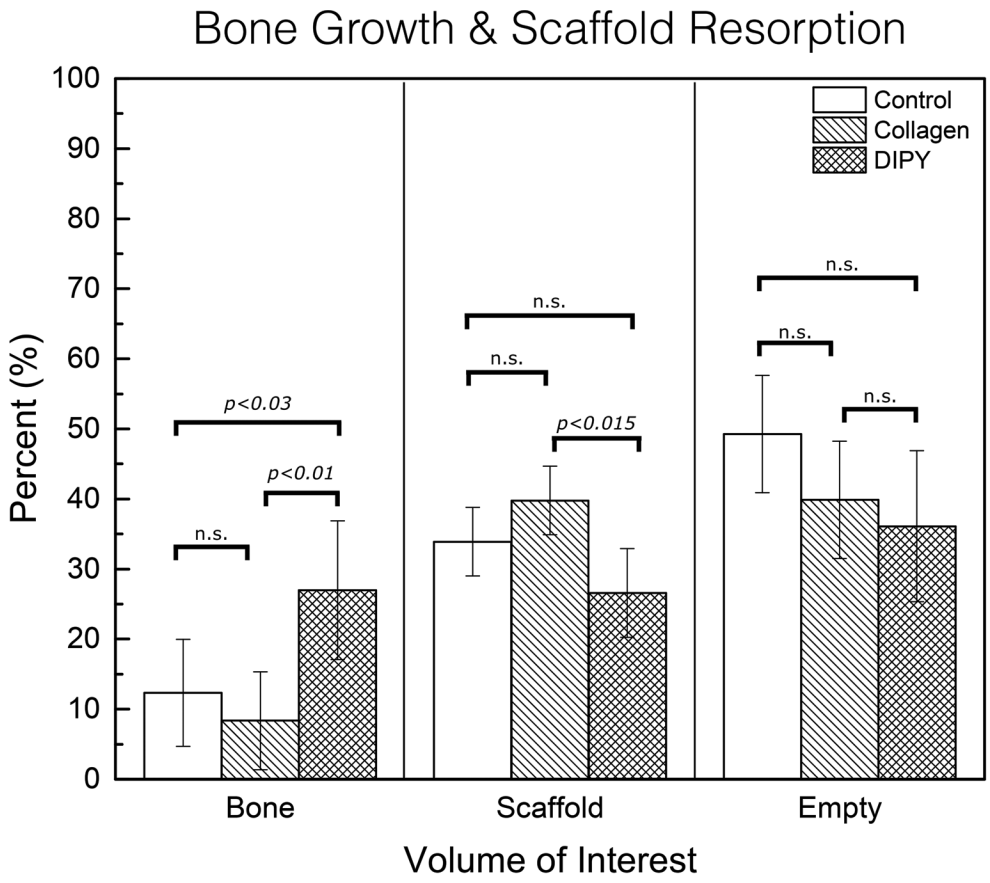

Figure 6:

Total volume for region of interest (scaffold construct, bone growth within scaffold construct, and porosity/potential space within scaffold termed empty space, all of which cumulatively add up to 100% of volume.

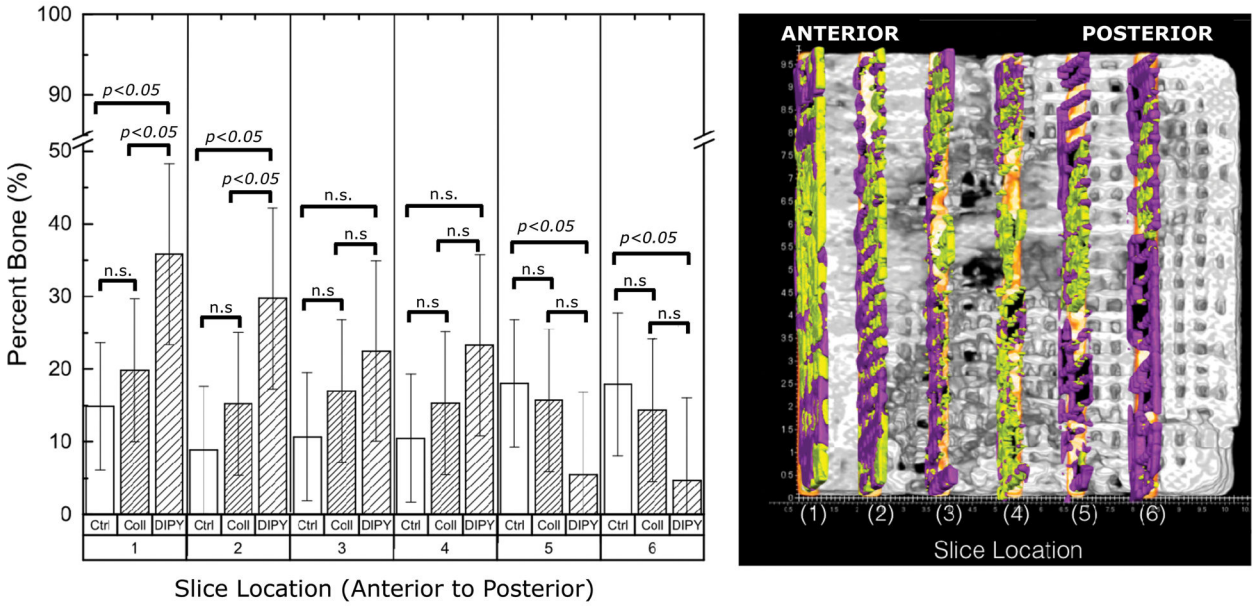

Figure 7:

Slice Analysis (a)Quantified bone regeneration within scaffold porosity from anterior (deepest aspect) to posterior (most exposed aspect) scaffold in 1.5 mm increments by experimental group. Slices were 0.25mm thick. Within each category (e.g. Ctrl, COLL, DIPY) different numbers of asterisks denote statistical differences that are significant (e.g. one asterisk is significantly different from two). All $p<0.05$. (b) AMIRA software depiction of slices selected for quantification. Bone is in yellow and scaffold is in purple.